Journal of the Korean Physical Society, Vol. 69, No. 6, September 2016, pp. 957∼961

Spatial and Temporal Measurements of Plasma/Gas Densities in a Capillary Gas-Cell for Laser-Plasma Accelerators

Inhyuk Nam, Minseok Kim, Seung-woo Lee, Dogeun Jang and Hyyong Suk*
Department of Physics and Photon Science, Gwangju Institute of Science and Technology, Gwangju 61005, Korea

(Received 28 December 2015, in final form 17 May 2016)

The measurement of the plasma density is of crucial importance in laser-plasma accelerators. We measured the spatial and the temporal plasma/gas densities in a capillary gas-cell by using the interferometric and the Raman scattering methods. By using transverse interferometry, we were able to measure directly the spatial distribution of the electron density between the entrance and the location of gas injection in the capillary, and we compared the result with that from a computational fluid dynamics (CFD) simulation. By using longitudinal interferometry along the capillary's axis, we were able to obtain the temporal evolution of the density of hydrogen gas. Furthermore, we used the stimulated Raman forward scattering method with a terawatt-level high-power laser beam for real-time measurement of the localized electron density inside the capillary. We found that the interferometry and the Raman scattering methods gave consistent results for the plasma density.

PACS numbers: 52.25.-b, 52.70.-m, 52.50.Jm, 41.75.Jv, 07.60.Ly
Keywords: Laser-plasma accelerator, Plasma diagnostics, Capillary gas-cell, Mach-Zehnder interferometry, Raman scattering
DOI: 10.3938/jkps.69.957

I. INTRODUCTION

The laser wakefield acceleration (LWFA) method has made it possible to produce highly relativistic electron beams in a centimeter-scale plasma [1]. Because of its great potential applications for high-energy particle acceleration and femtosecond X-ray generation, extensive studies have been performed [2,3]. For these applications, improved reproducibility and stability of the high-energy electron beams from LWFA are vital. If a stable electron beams is to be provided, the plasma source should provide a stable plasma density and the laser system should be stable because even a subtle fluctuation of the plasma density will cause a large change in the electron beam due to their nonlinear dependence.

In LWFA, so far, several types of plasma sources such as gas jets, gas-cells, and capillary's type gas-cells with/without electrical discharge, have been used. Among them, the capillary gas-cells most likely to produce stable electron beams because the plasma in the capillary hole is quite stable and homogeneous, because neither a shock wave nor shot-to-shot fluctuations occur there [4–6]. Hence, the characteristics of the capillary gas-cell were investigated by using the interferometry method and fluid dynamics simulations [7–9]. By using longitudinal interferometry along the capillary axis, J. Ju *et al.* obtained the temporal evolution of the gas density in a capillary gas-cell with a round cross section [8]. In their case, however, the detailed gas density profile from the entrance to the gas injection line was not measured and was uncertain. The density distribution in the up-ramp region, which severely affects the propagation of an intense laser beam, is very important as this region ultimately affects the output properties of the electron beam in LWFA. In recent years, most LWFA experiments are performed in the so-called "bubble regime" by using a high-power laser pulse with a normalized amplitude of $a_0 \geq 1$ [10], and the relativistic self-focusing effect plays a very important role, for example, in the generation of a laser-driven wake wave and the self-injection of the plasma electrons, in the density up-ramp region of the capillary.

In this paper, therefore, the density profile in the up-ramp region of the capillary was measured by using transverse interferometry, and the result is compared with the CFD simulation result. In addition to the detailed density information in the density up-ramp region, real-time information for the localized plasma density deep inside the capillary gas-cell is also very important for successful LWFA. The strong laser-plasma interaction deep inside the capillary hole can generate Raman forward scattering in the process of laser-plasma acceleration and the scattered light has information on the localized density at the location of the laser-plasma interaction. By measuring the frequency-shifted Stokes line from the Raman forward scattering, we can deduce

*E-mail: hysuk@gist.ac.kr

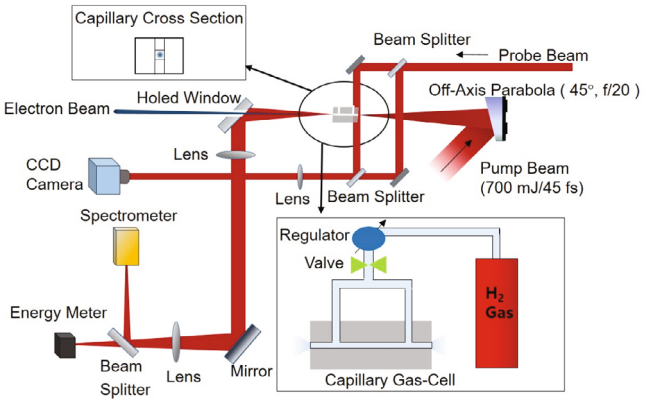

Fig. 1. (Color online) Experimental setup for the gas/plasma density measurement in a capillary gas-cell. The upper left inset shows a transverse cross section of the capillary gas-cell and the lower right inset shows its longitudinal cross section.

the plasma density [11]. In this paper, the result from a density measurement based on the Raman scattering method is presented.

II. EXPERIMENTAL SETUP

The capillary used in this experiment has a square cross-section with thick and thin sapphire plates as shown in the upper left inset of Fig. 1. The overall width and length of the sapphire plates are 4 mm and 15 mm, respectively, and the square hole has a width of 300 μm on each side. Hydrogen gas flows in the capillary hole through the gas-injection lines, with a width of 0.7 mm and a depth of 0.35 mm, that are carved on the surface of the thick plate by using a laser machining process.

Figure 1 shows a schematic diagram of the experimental setup to measure the plasma/gas density in the capillary gas-cell. In order to measure the density profile in the up-ramp region of the capillary, we used transverse interferometry. In this scheme, an intense pump laser beam with a pulse duration of 45 fs (700 mJ in energy/pulse, 800 nm in wavelength) was used to fully ionize the gas in the up-ramp region because measuring the phase shift from neutral hydrogen gas over a short distance of the cross-section is difficult due to the small refractive index of the gas. Then, a weak probe laser beam, which is divided from the pump laser beam is used for transverse interferometry to measure the density profile of the laser-induced plasma whose refractive index is much larger than that of the neutral gas. We can then assume that the density profile of the plasma is the same as that of the gas in the up-ramp region of the capillary.

To obtain the evolution of the temporal gas density in the capillary, we also used longitudinal interferometry along the capillary axis. The phase shift from the hydrogen gas over a capillary length of 15 mm can be measured, and the result will lead to the evolution of the gas density with time. In this experiment, continuous wave He-Ne laser (2 mW, 632 nm) in the laboratory was used to obtain the temporal density information. The fringe patterns formed by two interfering beams at the last beam splitter were then recorded by using an 8 bit charge-coupled device (CCD) at 60 Hz. As mentioned earlier, the amount of gas in the up and the down ramp regions can contribute to the total phase shift along the capillary axis. Therefore, we used the density profile measured in the up-ramp region by using transverse interferometry to deduce the gas density in the plateau region between the two gas injection lines.

In addition to the transverse and the longitudinal interferometric methods, the local plasma density in the plateau region of the capillary was directly measured by using the Raman forward scattering method. When an intense laser beam is focused in the plasma, the laser beam interacts with the plasma within the Rayleigh range, and forward Raman scatted radiation can be generated. Then, the plasma density can be deduced by measuring the frequency shift, which is easily measured with a spectrometer.

III. EXPERIMENTAL AND CFD SIMULATION RESULTS

1. CFD Simulations

Before the experimental work, we performed extensive two-dimensional (2D) CFD simulation studies by using the code ANSYS to design a capillary gas-cell, with the aim to obtain a spatial density distribution in the capillary gas-cell. The code numerically solves the Navier-Stokes equations, where the κ - ε model [12] is employed for turbulence consideration. Figure 2 shows a pressure distribution for an input pressure of 200 mbar in the capillary. The simulation result shows that the pressure is very homogeneous between the two gas inlets (*i.e.*, in the plateau region) and rapidly decreases near the capillary exit (*i.e.*, in the up-and the down-ramp regions). The gas filling efficiency depends on the cross-sectional area of the gas inlet, where the width is 0.7 mm and the depth is 0.35 mm. The result indicates that the gas filling efficiency increases as the cross section increases. As shown in Fig. 2(b), the pressure in the plateau region is 197 mbar for an input pressure of 200 mbar, which gives a filling efficiency of 98.5%, which means that the pressure of the plateau region is almost the same as the input pressure. In the up- and the down-ramp regions, the pressure is reduced rapidly, as can be imagined, and these regions contribute about 38% to the total phase shift in the gas-filled capillary.

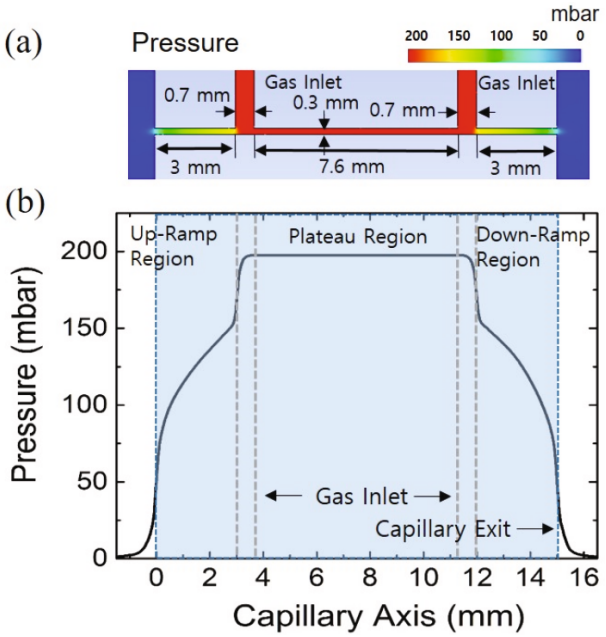

Fig. 2. (Color online) (a) 2-dimensional pressure distribution from the CFD simulation for a capillary gas-cell with an input pressure of 200 mbar and (b) its pressure profile along the axial direction in the capillary.

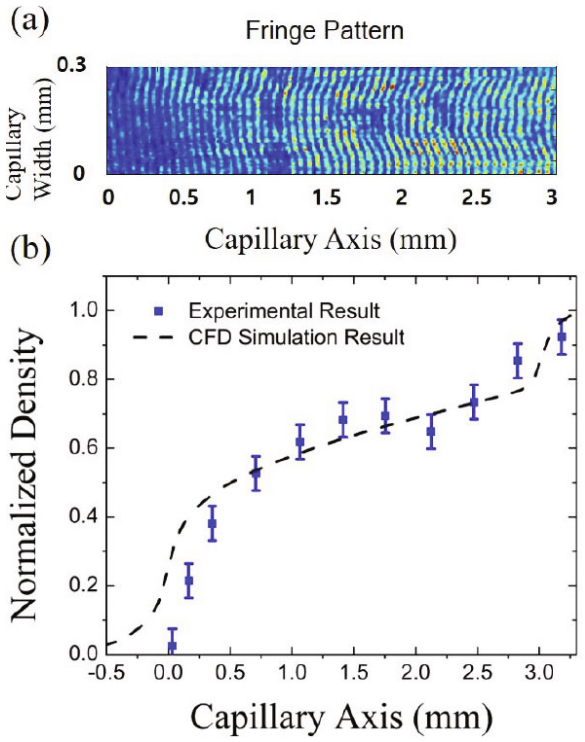

Fig. 3. (Color online) (a) Typical fringe pattern in the density up-ramp region of a capillary gas cell, measured by using transverse interferometry in the case of a backing pressure of 450 mbar. (b) Comparison of the electron density profiles from the transverse interferometry result and the CFD simulation result.

2. Interferometric Methods

In order to directly measure the spatial density profile in the up-ramp region, we used transverse interferometry. The laser pulse with a spot size of 30 μm (radius at $1/e^2$) was focused 1.5 mm away from the entrance of the capillary and generated a laser-produced plasma over a Rayleigh length of 2.7 mm. A laser pulse energy of $E >$ 300 mJ was used, and the intensity was calculated as $I = 4.7 \times 10^{17}$ W/cm^2, which was much higher than that of the ionization threshold for hydrogen ($I \geq 2 \times 10^{15}$ W/cm^2). Hence, a fully-ionized plasma can be formed locally near the focus, and the focus location can be moved along the longitudinal direction up to the gas inlet by moving the capillary. The probe beam, which is sampled from the pump pulse, is split into two beams in transverse interferometry, where one beam passes through the plasma 2 ps after the pump beam. The probe beam size is 5 mm (FHWM) so that the whole up-ramp region is covered by the probe laser beam at once.

Figure 3(a) shows a typical fringe pattern with the backing pressure of 450 mbar. The phase shift produced by the plasma over the capillary cross-section width d is given by

$$\Delta\varphi(x) = \frac{2\pi}{\lambda}\int_0^d [\eta(x,y) - 1]dy \ , \qquad (1)$$

where x is the transvers coordinate across the capillary hole, y is the longitudinal coordinate along the capillary axis, and λ is the laser wavelength. he refractive index of the plasma is given by $= \sqrt{(1 - \omega_{pe}^2/\omega_L^2)}$, where ω_{pe}, ω_L are the plasma and the laser frequencies, respectively. Then, the phase shift is given by

$$\Delta\varphi(x) = -r_e\lambda\int_0^d n(x)dy \ , \qquad (2)$$

where r_e is the classical electron radius. The electron density profile can be easily obtained from the phase shift by using the fringe analysis method without the Abel inversion, where the density profile is assumed to be a Gaussian distribution [13]. Figure 3(b) shows the measured plasma density profile in the up-ramp region near the capillary entrance, which indicates that the plasma density decreases sharply beyond the gas inlet (injection) line in the capillary.

In addition to measuring the plasma density near the capillary entrance by using transverse interferometry, we also obtained the temporal evolution of the gas density along the capillary axis. In this case, the longitudinal axis is long enough (1.5 cm) so that the phase shift of the hydrogen-filled capillary is large. Hence, this method can be used for a round cross-section-type capillary which is widely used in LWFA experiments. The phase-shift variation in time is caused by the variation of the refractive index of the gas integrated along the longitudinal direc-

tion of the capillary line and is given by

$$\Delta\varphi(t) = \frac{2\pi}{\lambda}\int_L [\eta(x,t)-1]dx \ , \quad (3)$$

where η is the refractive index of the neutral gas and L is the total length of the capillary. The refractive index is related with the gas density $n \cong (\eta-1)/\frac{3Am_H}{2}$, where A is the molecular refractivity and m_H is mass of the hydrogen. Then, the phase shift is given by

$$\begin{aligned}\Delta\varphi(t) &= \alpha\int_L n(t,x)dx \\ &= \alpha[2\int_{L_{ramp}} n(t,x)dx + n_p(t)L_{plateau}] \ , \quad (4)\end{aligned}$$

where $\alpha = 3\pi Am_H/\lambda = 4.09\times10^{-19}$ cm^{-2}, L_{ramp} and $L_{plateau}$ are the up- and the down ramp lengths, respectively, and n_p is the plateau density. The density profile in the up-/down-ramp region is required in order to calculate the plateau density. Thus, for the first term in Eq. (4), we used the directly measured result from the previous transverse interferometry experiment.

Figure 4(a) presents the temporal evolution of the plateau density. When the solenoid valve opened, the hydrogen gas was injected into the capillary gas inlet lines with a duration of 50 ms. The phase shift was recorded until the gas was completely removed from the capillary hole, which took about 10 seconds. The opening speed of the solenoid valve was only 2 ms which was negligible compared to the long opening time. As shown in the inset of Fig. 4(a), the capillary is completely filled with the gas within a 50 ms. Although the gas injection duration was increased up to a few hundred ms, the gas filling time did not change. This result indicates that the duration of gas injection can be decreased down to 50 ms in an LWFA experiment to minimize the vacuum pump load. Figure 4(b) shows the measured electron density as a function of the backing pressure, where longitudinal interferometry was used along the capillary axis. The dotted line is from the assumption that hydrogen in the capillary gas at the backing pressure is fully ionized by the high-power laser beam.

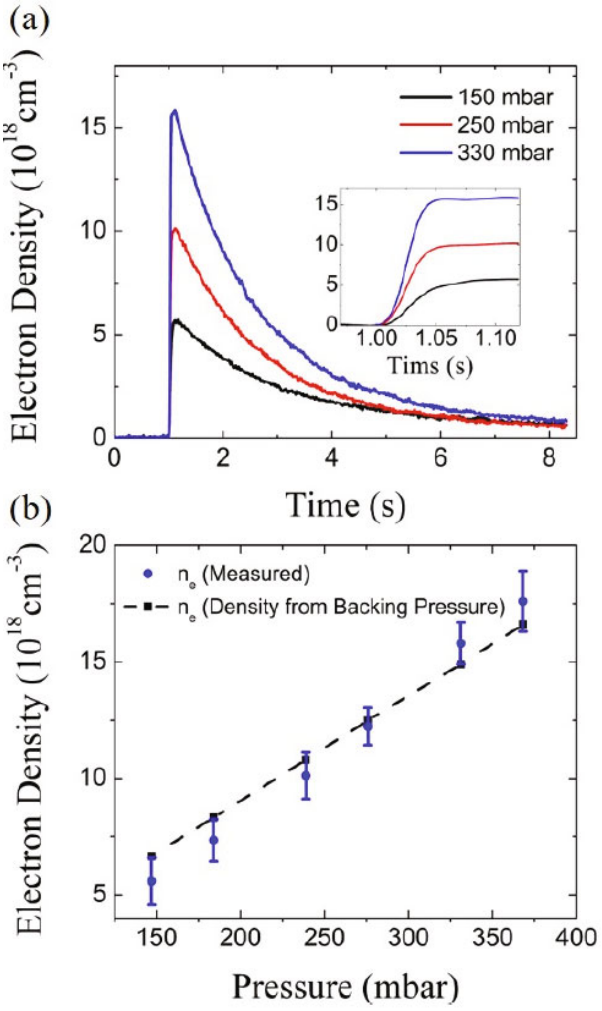

Fig. 4. (Color online) (a) Electron density evolution inside a capillary gas cell as a function of time for different backing pressures, measured by using longitudinal interferometry. (b) Electron density measured by using longitudinal interferometry as a function of the backing pressure in the capillary gas cell. The blue dots represent the measured density, and the black dashed-line represents the backing- pressure-based electron density under the assumption that the hydrogen gas is fully ionized by the high-power laser beam.

3. Stimulated Raman Scattering Method

For comparison with the interferometric methods, we measured the plasma density profile along the capillary axis by using Raman forward scattering. This method is very useful because it can provide density information during the laser-plasma experiments. The magnitude of the Raman instability is proportional to a pulse duration and intensity. In this experiment, the laser pulse with a peak power of $\sim$ 10 TW and a pulse duration of 45 fs was focused with a focal spot size of 21 $\times$ 22 μm^2 by an off-axis parabolic (OAP) mirror with an f-number of 20. By measuring the frequency shift $\omega_s = \omega_L - \omega_{pe}$ from Raman forward scattering, we were able to deduce the plasma density by using the plasma frequency $\omega_{pe} = \sqrt{n_e e^2/m_e\epsilon_0}$, where n_e and m_e are the plasma electron density and the electron mass, respectively. Figure 5(a) shows the frequency-shifted spectra including the plasma density information. For example, if the frequency shift is 94 nm in wavelength, the plasma density is calculated to be 2 $\times$ 10^{19} cm^{-3}. The experimental result shows that the wavelength shift decreases if the pressure is reduced. Figure 5(b) shows the measured electron density as a function of pressure. The dashed line represents the density calculated under the assumption that the hydrogen gas is fully ionized. This result is in agreement with

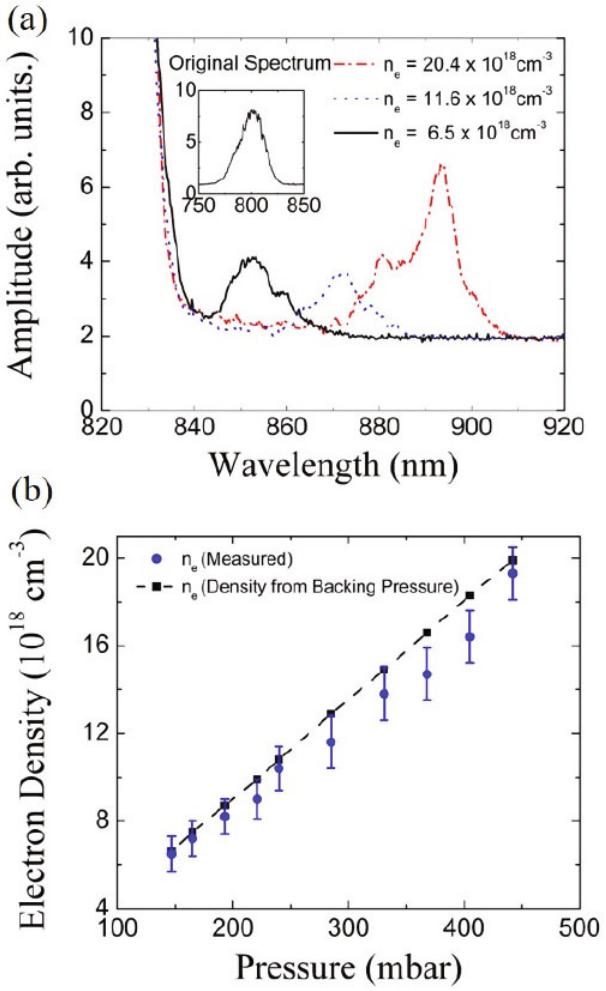

Fig. 5. (Color online) (a) Forward-scattered Raman spectra of the original high-power laser pulse, where Stokes lines are generated by the strong laser-plasma interaction. (b) Electron densities measured by using the Raman scattering method, where the blue dots represent the measured electron density and the black dashed-line represents the electron density based on the assumption that the hydrogen gas with a backing pressure is fully ionized by the high-power laser beam.

the density measured by using the interferometry, which is shown in Fig. 4(b).

IV. CONCLUSIONS

In conclusion, we measured the spatial and the temporal plasma/gas density in a capillary gas-cell by using the transverse and the longitudinal interferometric methods. We found that the density profile in the up-ramp region of the capillary gas-cell agreed with the CFD simulation result. Furthermore, the plasma density measured by using the stimulated Raman forward scattering method was also consistent with the interferometry result and can be used for real-time density measurement in laser-plasma acceleration experiments.

ACKNOWLEDGMENTS

This research was financially supported by the National Research Foundation of Korea (grant #: 2014M1A7A1A01030173) and by the Gwangju Institute of Science and Technology Top Brand Project (GIST TBP) program.

REFERENCES

[1] W. P. Leemans, A. J. Gonsalves, H.-S. Mao, K. Nakamura, C. Benedetti, C. B. Schroeder, Cs. Tóth, J. Daniels, D. E. Mittelberger, S. S. Bulanov, J-L. Vay, C. G. R. Geddes and E. Esarey, Phys. Rev. Lett. **113**, 245002 (2014).

[2] M. Fuchs, R. Weingartner, A. Popp, Z. Major, S. Becker, J. Osterhoff, I. Cortrie, B. Zeitler, R. Hörlein, G. D. Tsakiris, U. Schramm, T. P. Rowlands-Rees, S. M. Hooker, D. Habs, F. Krausz, S. Karsch and F. Grüner, Nat. Phys. **5**, 826 (2009).

[3] S. Kneip, C. McGuffey, J. L. Martins, S. F. Martins, C. Bellei, V. Chvykov, F. Dollar, R. Fonseca, C. Huntington, G. Kalintchenko, A. Maksimchuk, S. P. D. Mangles, T. Matsuoka, S. R. Nagel, C. A. J. Palmer, J. Schreiber, K. T. Phuoc, A. G. R. Thomas, V. Yanovsky, L. O. Silva, K. Krushelnick and Z. Najmudin, Nat. Phys. **6**, 980 (2010).

[4] J. Osterhoff, A. Popp, Z. Major, B. Marx, T. P. Rowlands-Rees, M. Fuchs, M. Geissler, R. Hörlein, B. Hidding, S. Becker, E. A. Peralta, U. Schramm, F. Grüner, D. Habs, F. Krausz, S. M. Hooker and S. Karsch, Phys. Rev. Lett. **101**, 085002 (2008).

[5] M. Hansson, L. Senje, A. Persson, O. Lundh, C-G. Wahlström, F. G. Desforges, J. Ju, T. L. Audet, B. Cros, S. Dobosz Dufrénoy and P. Monot, Phys. Rev. ST Accel. Beams **17**, 031303 (2014).

[6] I. Nam, M. Kim, T. H. Lee, S. W. Lee and H. Suk, Curr. Appl. Phys. **15**, 468 (2015).

[7] A. J. Gonsalves, T. P. Rowlands-Rees, B. H. P. Broks, J. J. A. M. van der Mullen and S. M. Hooker, Phys. Rev. Lett. **98**, 025002 (2007).

[8] J. Ju and B. Cros, J. Appl. Phys. **112**, 113102 (2012).

[9] C. Ciocarlan, S. M. Wiggins, M. R. Islam, B. Ersfeld, S. Abuazoum, R. Wilson, C. Aniculaesei, G. H. Welsh, G. Vieux and D. A. Jaroszynski, Phys. Plasmas **20**, 093108 (2013).

[10] W. Lu, M. Tzoufras, C. Joshi, F. S. Tsung, W. B. Mori, J. Vieira, R. A. Fonseca and L. O. Silva, Phys. Rev. ST Accel. Beams **10**, 061301 (2007).

[11] M. D. Perry, C. Darrow, C. Coverdale and J. K. Crane, Opt. Lett. **17**, 523 (1992).

[12] W. Jones and B. Launder, Int. J. Heat Mass Transfer **15**, 301 (1972).

[13] C. Kim, G. H. Kim, J. U. Kim, I. S. Ko and H. Suk, Rev. Sci. Instrum. **75**, 2865 (2004).